Comparison of Observed Temperature and Salinity Changes in the Indo-Pacific with Results from the Coupled Climate Model HadCM3: Processes and Mechanisms*

HELENE T. BANKS

Hadley Centre for Climate Prediction and Research, Met Office, Bracknell, Berkshire, United Kingdom

NATHANIEL L. BINDOFF

Antarctic Co-operative Research Centre, Hobart, Australia

(Manuscript received 28 December 2001, in final form 2 July 2002)

ABSTRACT

Observed changes in temperature and salinity properties on isopycnals across hydrographic sections throughout the Indo-Pacific are compared with the changes modeled by the coupled climate model, HadCM3. Observations show cooling and freshening on isopycnals in midlatitudes, and there is quantitative agreement between modeled and observed water mass changes on five out of six zonal sections. The full Indo-Pacific pattern of change in the climate model is examined and it is discovered that the pattern of cooling and freshening on isopycnals in midlatitudes, with warming on isopycnals at high latitudes, may be thought of as a fingerprint of anthropogenic forcing. The water mass changes are related to changes in the surface fluxes and it is found that surface warming is the dominant factor in producing water mass changes, although changes in the freshwater cycle are important in the formation zone for Antarctic Intermediate Water. The coupled model has a low-amplitude, low-frequency (100-yr period) internal mode related to the anthropogenic fingerprint. Further observations are required to measure the amplitude of the internal mode as well as the anthropogenically forced mode.

1. Introduction

Over the last 40 years there have been a number of observations of temperature and salinity properties of subsurface water masses in the Indo-Pacific (Bindoff and Church 1992; Johnson and Orsi 1997; Wong et al. 1999; Bindoff and McDougall 2000). These observations show that in mode and intermediate waters, the water mass properties have become colder and fresher on isopycnals over this period. Changes in temperature and salinity on isopycnals reflect changes in surface forcing, yet it may be extremely difficult to link observed subsurface changes with observed changes in surface forcing. Inherent noise and natural variability of the ocean surface makes direct measurements of surface fluxes difficult and, as a consequence, measurements of long-term changes in surface fluxes are affected by low signal-to-noise ratios. Subsurface ocean temperature and salinity fields can act to integrate surface fluxes and because of relatively low variability in the subsurface ocean (as shown by Banks and Wood 2002), high signal-to-noise ratios should be found there. There has been much speculation about whether the observed changes are a natural cycle of the climate system or forced by anthropogenic climate change (Wong et al. 1999), but, given that subsurface ocean measurements only go back approximately 60 years (Levitus et al. 1998), it is virtually impossible to ascertain this from ocean observations themselves.

Coupled ocean–atmosphere models have become sufficiently sophisticated in the last five years that artificial flux adjustments that may have hindered their realism are now no longer necessary (Gordon et al. 2000). These models are now producing simulations of the last century based on historical records of atmospheric constituents with projections into the future based on scenarios and are used to give policy advice through the Intergovernmental Panel on Climate Change (IPCC) process (Houghton et al. 2001). In order to establish the credibility of models such as these, it is important to validate their simulations of the last century against observed historical changes in the climate system, both in the atmosphere and the ocean. Levitus et al. (2001) and Barnett et al. (2001) have shown that two coupled models can produce observed trends in ocean heat content. Our work aims to look at whether one coupled model

* This study contributes to the World Ocean Circulation Experiment.

Corresponding author address: Dr. Helene T. Banks, Hadley Centre for Climate Prediction and Research, Met Office, London Road, Bracknell, Berkshire RG12 2SY, United Kingdom.
E-mail: helene.banks@metoffice.com

TABLE 1. Modern and historical data used in the comparison.

Zonal section	Modern (yr)	No. of casts	Historical (yr)	No. of casts	Std dev (yr)	Time difference (yr)
47°N	1985	299	1966	299	5.0	19
24°N	1985	156	1970	509	5.5	15
10°N	1989	213	1969	400	6.0	20
17°S	1994	294	1967	706	5.0	30
32°S	1987	109	1962	451	10.0	25
43°S	1989	72	1967	18	<1	22

can produce the observed changes in temperature and salinity on isopycnals. Beyond validation, in a coupled model it is possible to diagnose surface forcing and, therefore, to try to understand the processes and mechanisms by which subsurface oceanic changes may occur.

This paper aims to address three questions: 1) Can a coupled climate model reproduce observed water mass changes in the Indo-Pacific? 2) Are observed changes anthropogenically forced or a signal of internal variability? 3) What atmospheric changes drive the observed subsurface water mass changes? We will first describe observations from the Indo-Pacific over the last century and simulations of a state-of-the-art coupled climate model, the third Hadley Centre Coupled Ocean–Atmosphere General Circulation Model (HadCM3; section 2). We will then compare observed changes in temperature and salinity with those simulated by the coupled climate model (section 3). In section 4 we will find the pattern of change in the coupled model that may be thought of as a fingerprint of anthropogenic forcing, and in section 5 we will relate the subsurface fingerprint to the changes in surface fluxes. Finally, in section 6 we will draw conclusions.

2. Data and methods

a. The data

We compare the output of the model with the observed differences in temperature and salinity in the deep ocean (Table 1). These differences are constructed from a variety of datasets and analyses (Bindoff and Church 1992; Bindoff and McDougall 1994, 2000; Wong et al. 2001). The historical data are primarily obtained from J. Reid and A. Mantyla (1994, personal communication) and from the *Southern Ocean Atlas* (Gordon et al. 1982) for both the Indian and Pacific Oceans. The hydrographic data from these atlases are mainly Nansen bottle data. The recent hydrographic data come from the World Ocean Circulation Experiment (WOCE) and are available from the World Hydrographic Program Office (WHPO; see online at http://whpo.ucsd.edu). These WOCE data are all CTD data calibrated against salinity analyses from water samples taken through the whole water column. Typical accuracies of the CTD temperature and salinity data are 0.002°C and 0.003 psu. The historical data are interpolated to the location of each cast from the recent hydrographic profiles using objective methods (Bretherton et al. 1976; Roemmich 1983; Bindoff and Wunsch 1992). The observed differences along these sections (Table 1) are distributed over both the Pacific and Indian Oceans (Fig. 1). The best coverage is of the Pacific basin, although the South Pacific is less well covered. These observed differences have been interpreted in earlier papers (listed above) but are now compared with the HadCM3 model for the first time.

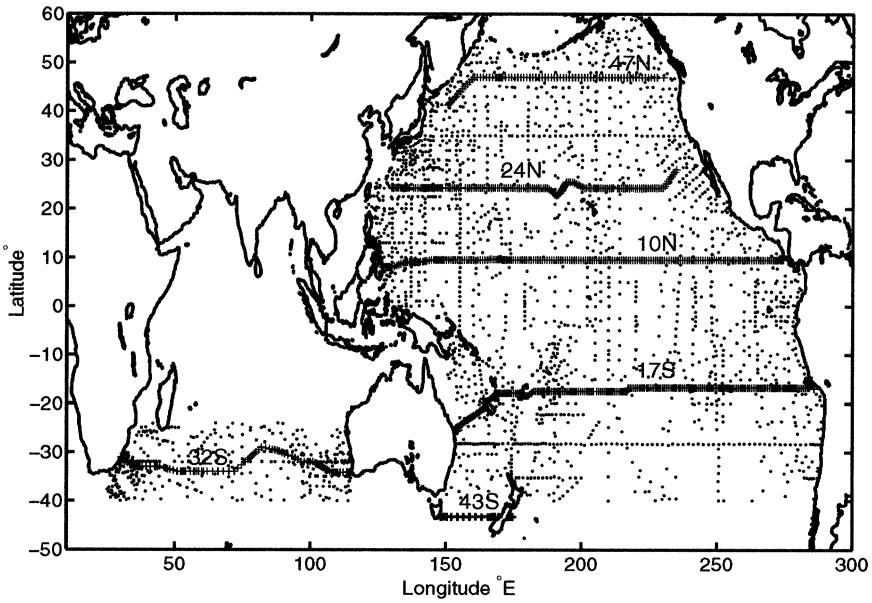

FIG. 1. The locations of the historical and modern data used to compare with the results from the coupled ocean–atmosphere model (HadCM3).

b. Numerical model

The model we will look at here is the coupled ocean–atmosphere model, HadCM3 (Gordon et al. 2000), developed at the Hadley Centre. The major differences between this coupled model and the previous version (Johns et al. 1997) occur in the ocean component, which has higher horizontal resolution and employs the Gent and McWilliams (1990) scheme to represent mixing due to eddies. The introduction of these and other improvements meant that the coupled model no longer needed artificial flux adjustments to prevent the model drifting to an unrealistic state and exact fluxes are exchanged between the atmosphere and the ocean on a daily basis. The ocean component of the model is based on the Cox (1984) model with a horizontal resolution of 1.25° in both the north–south and east–west direction and 20 vertical levels. The reader is referred to Gordon et al. (2000) for details of the model.

Here we will examine two experiments; firstly, the control experiment (CTL) and secondly an anthropogenic climate change experiment B2. CTL is initialized with the temperature and salinity of the ocean given by the climatology of Levitus and Boyer (1994) and with both the atmosphere and ocean at rest. While the oceanic and atmospheric heat budgets come into balance within 10 yr in CTL (Gordon et al. 2000), this is not the case for the freshwater budgets, which require a timescale of the order of 300–400 yr to come into balance (Pardaens et al. 2001, manuscript submitted to *Climate Dyn.*, hereafter PBGR). Since any imbalance will directly affect the salinity structure of the ocean, this means that the water mass properties must have a similar timescale to the salinity field to reach a quasi equilibrium. For this reason, in this paper we will only look at water mass properties from year 370 onward.

Experiment B2 is initialized at year 370 of CTL. The B2 is a climate change experiment with imposed anthropogenic changes of well-mixed greenhouse gases, tropospheric and stratospheric ozone and sulphate aerosols, and is described in detail by Johns et al. (2001). The B2 is forced using historical emissions and concentrations from 1859 until the present, then the IPCC B2 scenario until 2100. Experiment B2 has previously been used by Banks et al. (2000) and Banks and Wood (2002) to look at changes in water mass properties. A simpler experiment with HadCM3 based on 2% increase per year in carbon dioxide was used by Banks et al. (2002) to understand the causes of change in Subantarctic Mode Water in the Indian Ocean. The present paper is the first to *quantitatively* compare HadCM3 and observations throughout the Indo-Pacific and in its examination of the basinwide modes of the Indo-Pacific.

3. Comparison of observed changes and coupled model changes

a. Qualitative comparison of modeled and observed temperature–salinity properties

Figure 1 shows the location of the observations used in this study (Wong et al. 1999). The dates of the observations are described in Table 1. It should be noted that the historical data are interpolated onto the location of the modern sections and have an associated error bar to account for the effects of mesoscale variability. We will use the uncertainties later. For the model data we have extracted zonal sections from the annual means of the years of the historical and modern observations at the same latitudes as the observed sections. We have calculated error bars for the model to account for the uncertainty in the date of the historical data and short-term variability of the model. This is based on the standard deviation of 5-yr differences in B2.

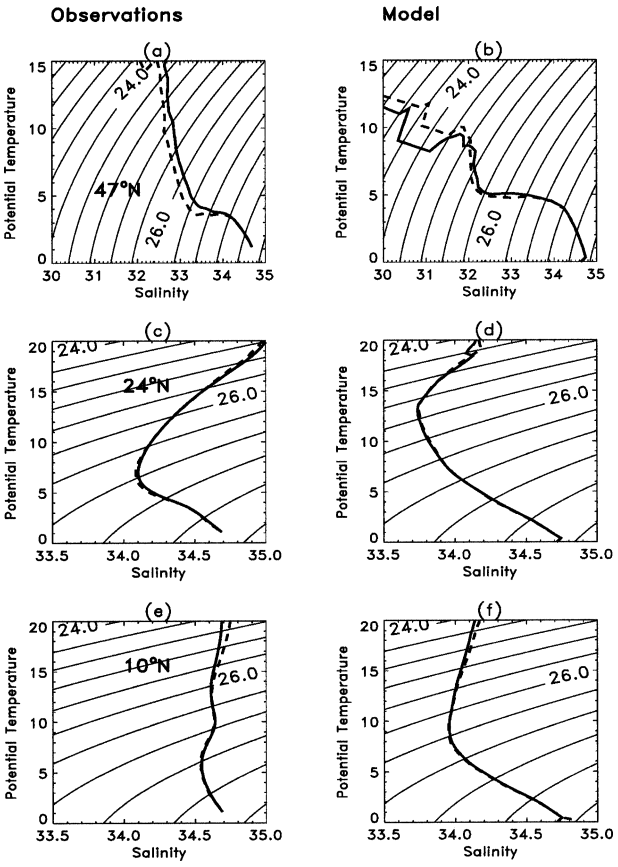

FIG. 2. Temperature–salinity diagrams showing the Southern Hemisphere section average water mass changes found in both (a), (c), (e) the observations and (b), (d), (f) in the HadCM3 anthropogenic climate change experiment (B2) of HadCM3 for the period shown in Table 1. (a), (b): 17°S; (c), (d): 32°S; and (e), (f): 43°S. The continuous lines are the old water mass characteristics, and the dashed lines are the new characteristics. The reader is referred to Fig. 4 to examine the changes in detail.

Figure 2 shows temperature–salinity diagrams from both the modern and historical times for both the observational data and the modeled data at the three southern sections; 43°, 32°, and 17°S. The bold lines denote the historical temperature–salinity profile, while the dashed lines denote the modern profile. In each case, the modeled and observed temperature–salinity profiles are qualitatively similar; in each profile there is a well-

TABLE 2. Potential density (kg m^{-3}) of water masses in both model and observations. Note that for the section at 47°N we take surface to be the upper limit of the zone of almost homogeneous salinity (see Figs. 3a and 3b).

Section	Water mass	Observed	Modeled
43°S	Surface	23.2	24.8
	Salinity max	26.6	25.4
	AAIW	27.4	26.2
	Deep	28.0	28.0
32°S	Surface	23.2	22.8
	Salinity max	26.0	24.8
	AAIW	27.4	26.4
	Deep	28.0	28.0
17°S	Surface	23.2	20.9
	Salinity max	24.4	24.4
	AAIW	27.0	26.2
	Deep	27.8	28.0
10°N	Surface	23.2	21.4
	NPIW	27.2	26.4
	Deep	28.0	27.8
24°N	Surface	23.2	23.1
	NPIW	26.8	25.2
	Deep	27.8	27.8
47°N	Surface	24.0	24.8
	NPIW	26.4	25.6
	Deep	27.8	27.8

defined salinity minimum denoting Antarctic Intermediate Water (AAIW). In the observations the minimum occurs at approximately 34.5 psu, 5°C, while in the model the minimum occurs at approximately 34 psu, 9°C. In both the observations and the model, below the salinity minimum, salinity increases to deep water (before decreasing in bottom water), while above the salinity minimum, salinity increases to reach a maximum before decreasing to the surface. For each section, Table 2 shows the density of the four water masses [surface, salinity maximum, AAIW (salinity minimum), and deep water] in both the observations and the model. The temperature–salinity diagrams are not quantitatively similar because in the coupled model, the ocean adjusts to balance the surface fluxes given by the atmospheric model. In the upper 1000 m, it takes about 400 yr for the temperature and salinity properties to reach a quasi equilibrium. Fortunately the observed and modeled temperature–salinity (T–S) diagrams are qualitatively similar, so we can still compare the water masses.

Figure 3 shows similar diagrams for the northern sections. At 10°N, the observations show a salinity minimum associated with North Pacific Intermediate Water (NPIW) at 34.5 psu, 6°C, while the model has a salinity minimum at 33.8 psu, 9°C. At 24°N, the salinity minimum is at 34.1 psu, 7°C in the observations and 33.7 psu, and 13°C in the model. At 47°N, both the modeled and observed temperature–salinity diagrams have a different shape to profiles farther south. This is because at this latitude we are in the center of the formation region for NPIW. This is identifiable by the ''corner'' in the T–S profile. This corner occurs at 33.3 psu, 4°C in the observations, and 32.5 psu, 5°C in the model. The densities of the significant water masses in the northern sections are also shown in Table 2.

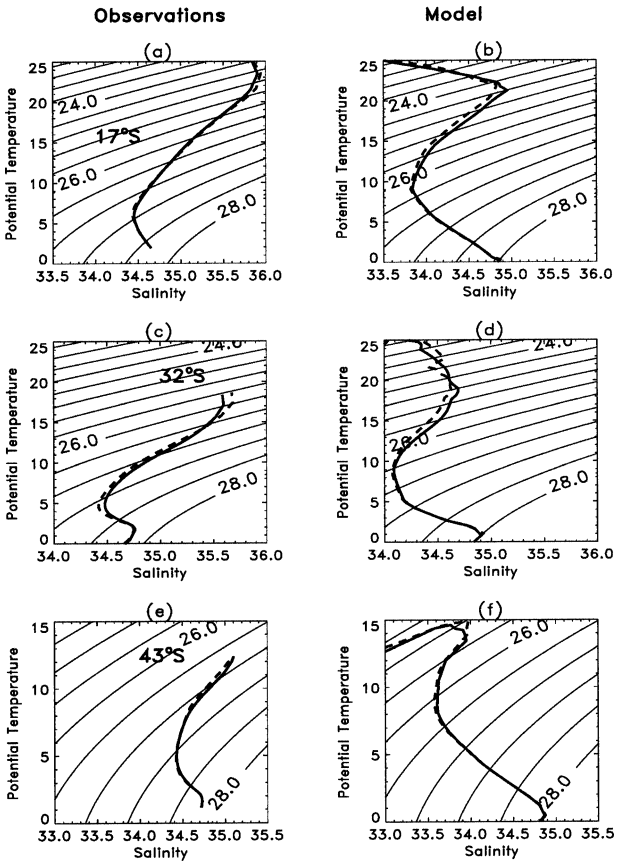

FIG. 3. The Northern Hemisphere average water mass changes found in both (a), (c), (e) the observations and (b), (d), (f) in the HadCM3 anthropogenic climate change experiment (B2) of HadCM3 for the period shown in Table 1. (a), (b): 47°N; (c), (d): 24°N; and (e), (f): 10°N. The continuous lines are the old water mass characteristics, and the dashed lines are the new characteristics. The reader is referred to Fig. 4 to examine the changes in detail.

b. *Qualitative comparison of modeled and observed changes*

From Fig. 2 we can see that at 43°S, in both the observations and the model, the water masses above AAIW became colder and fresher along isopycnals. A similar freshening occurs at 32°S, with waters at the shallow salinity maximum becoming warmer and saltier on isopycnals. At 17°S, although the observed changes seem fairly small, compared to the modeled changes, we can see a similar pattern emerging from both the model and the observations around AAIW.

In the Northern Hemisphere (Fig. 3), we can see subtropical waters becoming warmer and saltier on isopycnals at 10°N while NPIW becomes colder and fresher. At 24°N, NPIW becomes colder and fresher in the observations and warmer and saltier in the model, while subtropical waters become colder and fresher in both

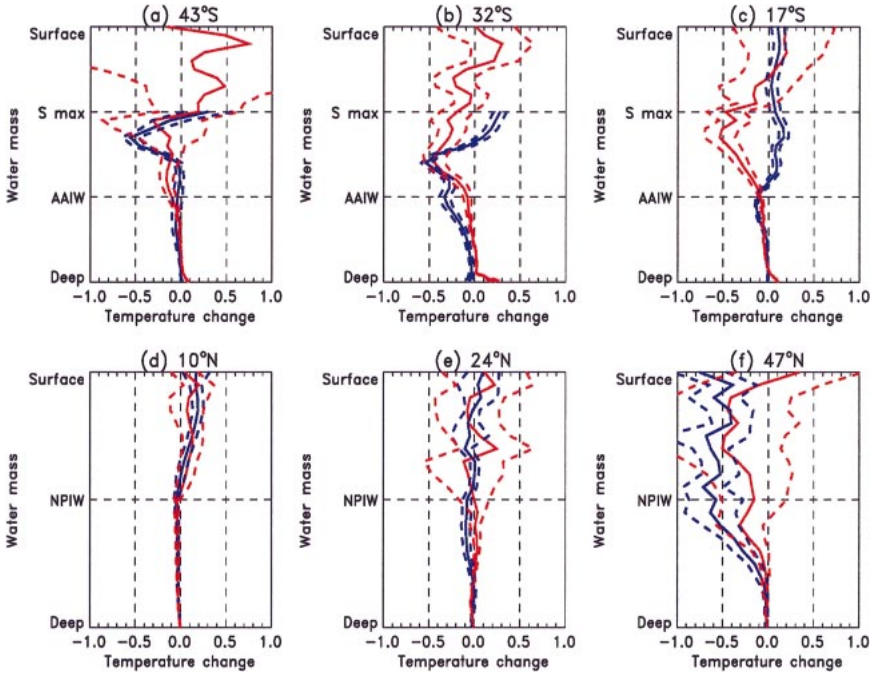

FIG. 4. Potential temperature changes on isopycnals from HadCM3 anthropogenic climate change experiment (B2) (red) and observations (blue). Dashed lines denote the error bars.

the model and the observations. At 47°N, both the observations and model show cooling and freshening on isopycnals around the core of NPIW.

c. Quantitative comparison of modeled and observed changes

As we can see from Figs. 2 and 3, it is not straightforward to make a quantitative comparison of observed and modeled water mass changes on isopycnals because of the different absolute properties of water masses. However, because we can clearly identify the same water masses in both the observations and model, we believe that it is worthwhile to make a quantitative comparison of changes in each water mass. The method we have employed is new and innovative, but the inspiration came from the application of fuzzy logic (Guiot et al. 1999). The idea behind the approach is to look for similarities between profiles and allow some offset in the positions of similar features.

For both the model and the observations, we can define a potential temperature change on isopycnals, $\theta'(\sigma)$, where θ' is the potential temperature change and σ is the potential density. If we compare the observed change, $\theta'_{\text{obs}}(\sigma)$, with the modeled change at the same density, $\theta'_{\text{mod}}(\sigma)$, the comparison will be meaningless because water masses are at different densities in the model and the observations. To make a meaningful comparison, we will interpolate θ'_{obs} and θ'_{mod} onto a new ''water mass axis'' that we will now define. In Table 2 we defined the principal water masses for each section in the model and the observations (surface, salinity maximum, AAIW/NPIW, and deep water). For the Southern Hemisphere sections there are four water masses ($n_{\text{wm}} = 4$), while for the Northern Hemisphere sections there are three water masses ($n_{\text{wm}} = 3$). We will call the water mass, wm(i), where $i = 0 \cdots n_{\text{wm}} - 1$. The density of water mass, wm(i), in the observations is $\sigma_{\text{obs}}[\text{wm}(i)]$ and in the model is $\sigma_{\text{mod}}[\text{wm}(i)]$. So for each water mass we can compare $\theta'_{\text{obs}}\{\sigma_{\text{obs}}[\text{wm}(i)]\}$ with $\theta'_{\text{mod}}\{\sigma_{\text{mod}}[\text{wm}(i)]\}$.

We can now take this one step further and interpolate the continuous profiles as a function of density to continuous profiles as a function of water mass. We define a water mass coordinate, l, to lie between 0 and $\lambda(n_{\text{wm}} - 1)$, where λ is a ''resolution factor.'' Here we will take λ to be equal to 10. We chose this value of λ because this gave a resolution comparable with the original data. Here l is defined as

$$l = \lambda i + j, \tag{1}$$

where $i = 0 \ldots n_{\text{wm}} - 2$ and $j = 0 \ldots \lambda$. We can then calculate the density at a particular l as

$$\sigma(l) = \sigma[\text{wm}(i)] + \frac{j\{\sigma[\text{wm}(i+1)] - \sigma[\text{wm}(i)]\}}{\lambda}. \tag{2}$$

The potential temperature change at water mass coordinate l is then simply $\theta'[\sigma(l)]$. We can then make a comparison between the observations and the model by comparing $\theta'_{\text{obs}}[\sigma_{\text{obs}}(l)]$ with $\theta'_{\text{mod}}[\sigma_{\text{mod}}(l)]$.

Figure 4 shows the potential temperature changes on isopycnals plotted against a water mass axis from both the model and observations. We have included error bars

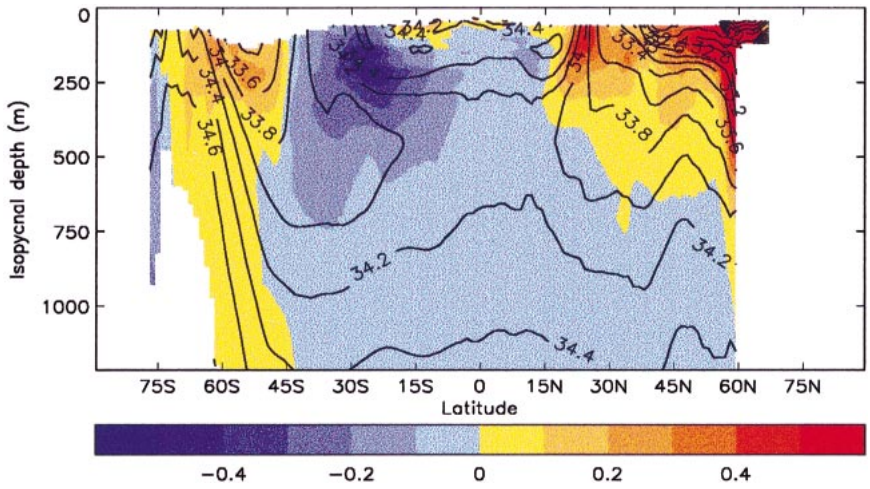

FIG. 5. Indo-Pacific zonal average potential temperature change on isopycnals from HadCM3 anthropogenic climate change experiment (B2) between 1959–68 and 1989–98. The changes on isopycnals have been regridded onto pressure surfaces using the mean depth of each isopycnal surface. Contours show the zonal average salinity field.

(as mentioned earlier) on both the modeled and observed changes. At 43° and 32°S, both the model and observations show cooling between AAIW and the salinity maximum. This is the part of the water column where Subantarctic Mode Water (SAMW) is found. At these latitudes the observed and modeled changes are of a similar magnitude. At 17°S, the observations show a weak cooling (approximately 0.1°C) around the salinity minimum associated with AAIW, while the modeled cooling is approximately 0.5°C and higher in the water column, around the salinity maximum (this difference can also be seen in Fig. 2). The difference between the model and observations cannot be explained by mesoscale or interannual variability as it lies outside the error bars of both the model and observations. In the Northern Hemisphere, although the changes at 10°N are weak in both the model and the observations, there is general agreement between the two. At 24°N, the comparison shows differences in the direction of the changes but the interannual variability (as shown by the model error bars) is large enough to contribute toward this difference except at depth. At 47°N, the observations and the model both show cooling of a similar magnitude through the water column.

In summary, for five out of six sections there is quantitative agreement between the changes in the modeled and observed water masses, which suggests that the model is capable of simulating the observed large-scale pattern of change.

4. The fingerprint of anthropogenic forcing in the Indo-Pacific

In the previous section we showed that the coupled model is able to capture the large-scale signal of cooling and freshening on isopycnals over the last 30 yr, as seen in the observations. In this section we aim to use the coupled model to see if the pattern we have seen is a signal of anthropogenic climate change or whether it is simply part of the internal variability of the climate system.

Figure 5 shows the zonally averaged change in temperature on isopycnals for the Indo-Pacific between the decadal means of 1959–68 and 1989–98 in the anthropogenic climate change (B2) model run. We choose a 30-yr period because this is a timescale typical of the separation time for observations (as seen in Table 1). By taking the difference of decadal averages we can eliminate variability on the interannual timescale. It shows that the water column has become warmer (and saltier) at high latitudes (poleward of 45°). Cooling (and freshening) originates from the surface in the Southern Hemisphere subtropics and extends below the surface into the Northern Hemisphere. In the Tropics the surface becomes warmer (and saltier) and in the Northern Hemisphere subtropics the water column has also become warmer (and saltier). In the Southern Hemisphere this pattern is similar to that shown by the earlier model–data comparison. In addition, although changes in the high latitudes have been poorly sampled in the observations, there is evidence to suggest that warming on isopycnals, as seen in the coupled model, is occurring (Aoki 1997; Aoki et al. 2001, manuscript submitted to *J. Geophys. Res.*). In the Northern Hemisphere the pattern is somewhat different to that seen earlier with less cooling and freshening apparent. This underlines the larger interannual and interdecadal variability in the Northern Hemisphere compared to the Southern Hemisphere, as suggested by the results of Banks et al. (2000). We call the pattern of change described above the asymmetric pattern and examine both CTL and B2 to see whether it is a signal of anthropogenic change.

We take the asymmetric pattern shown in Fig. 5 to be $P(x)$, where $x = 1 \ldots n$ is the position in latitude–depth space. From the CTL run we will take the time series of every (overlapping) 30-yr zonal average Indo-Pacific change of salinity on isopycnals. The differences are created by shifting the 30-yr period by 1 yr at a time. Since temperature and salinity changes on isopycnals are compensating it does not matter whether we choose to look at temperature or salinity. This is a representation of the changes due to internal variability of the coupled system. We will call this time series $I(x, t)$, where t denotes the time of the first year in the 30-yr difference. In addition, we will also take from B2 the time series of every 30-yr zonal average Indo-Pacific change of salinity on isopycnals. This is a representation of the changes due to anthropogenic forcing and we will call this time series $A(x, t)$.

We will then project both our time series of differences [$I(x, t)$ and $A(x, t)$] onto the asymmetric pattern [$P(x)$] to create time series $u(t)$ and $v(t)$ (see, e.g., Santer et al. (1995). These time series are calculated:

$$u(t) = \frac{\sum_{x=1}^{n} I(x, t)P(x)}{\sum_{x=1}^{n} P(x)P(x)} \quad (3)$$

$$v(t) = \frac{\sum_{x=1}^{n} A(x, t)P(x)}{\sum_{x=1}^{n} P(x)P(x)}. \quad (4)$$

Figure 6a shows u as a function of time. The internal variability u shows no significant drift over time and has periods that are correlated and anticorrelated with the asymmetric pattern but is essentially a random time series. Based on a one-tailed test (since we are looking for a positive correlation with the search pattern), the 5% significance level in the distribution of u is 0.5 (the time series has 31 degrees of freedom). This value is highlighted in Fig. 6a. The time series of v (Fig. 6b) shows that before 1950 there is no strong correlation with the asymmetric pattern. After 1950 the anthropogenic changes show a much redder spectrum with distinct periods of correlation with the asymmetric pattern; starting in approximately 1960, 2000, and 2050. Examining the time series of u and v suggests that CTL has no significant correlation with the asymmetric pattern and while the pattern becomes more common as anthropogenic forcing increases it is not dominant. To try and establish what pattern occurs when the projected values are low we will look at the 30-yr difference pattern starting in the 1990s.

Figure 7g shows the zonally averaged change in temperature on isopycnals between the decadal means of 1989–98 and 2019–28 from the anthropogenic climate change run (B2). This shows a pattern similar in many ways to that seen in Fig. 5 but with greater symmetry between the Northern and Southern Hemispheres and, in particular, cooling (and freshening) of the water column in the northern subtropics. We will call this the symmetric pattern and note that this pattern is qualitatively very similar to that seen in the observations. If we now repeat the projection of all the 30-yr differences onto the symmetric pattern, we get a somewhat different picture. Figure 8a shows that in the internal variability of the coupled system this pattern (although weak) does show some signs of low-frequency variability with a timescale of approximately 100 yr. Figure 8b shows, however, that the symmetric pattern is the dominant signal of anthropogenic forcing in the Indo-Pacific; all 30-yr changes starting from about 1960 exceed the 5% significance level from the internal variability. This suggests that the large-scale pattern of change seen in the observations of cooling and freshening on isopycnals in the subtropics of both hemispheres with warming (and salinification) occurring near the surface, may be thought of as a fingerprint of anthropogenic climate change in the ocean.

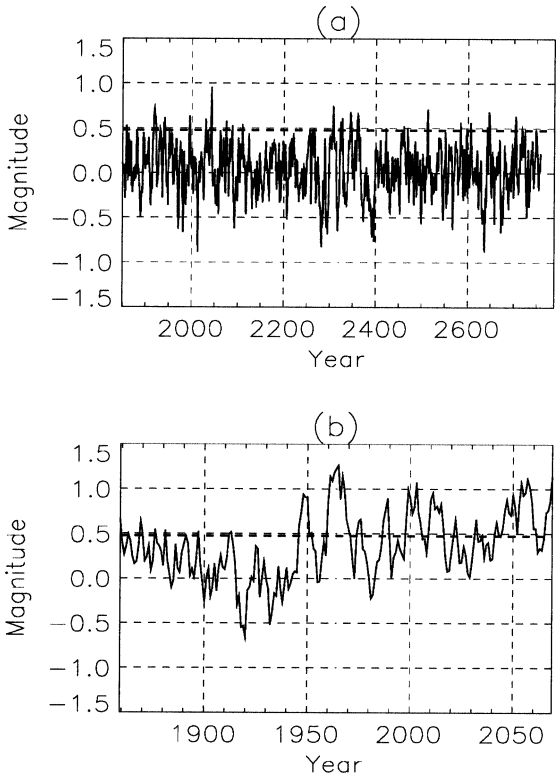

FIG. 6. Time series of the correlation of 30-yr changes in (a) CTL and (b) B2 projected onto the difference pattern from 1989 to 1998 minus 1959 to 1968. The 5% significance level from the CTL distribution is marked as the dashed line in both (a) and (b). Please note the different time axis in (a) and (b).

5. Mechanisms for the fingerprint

In this section we will focus on the fingerprint pattern seen in the coupled model. As discussed in the intro-

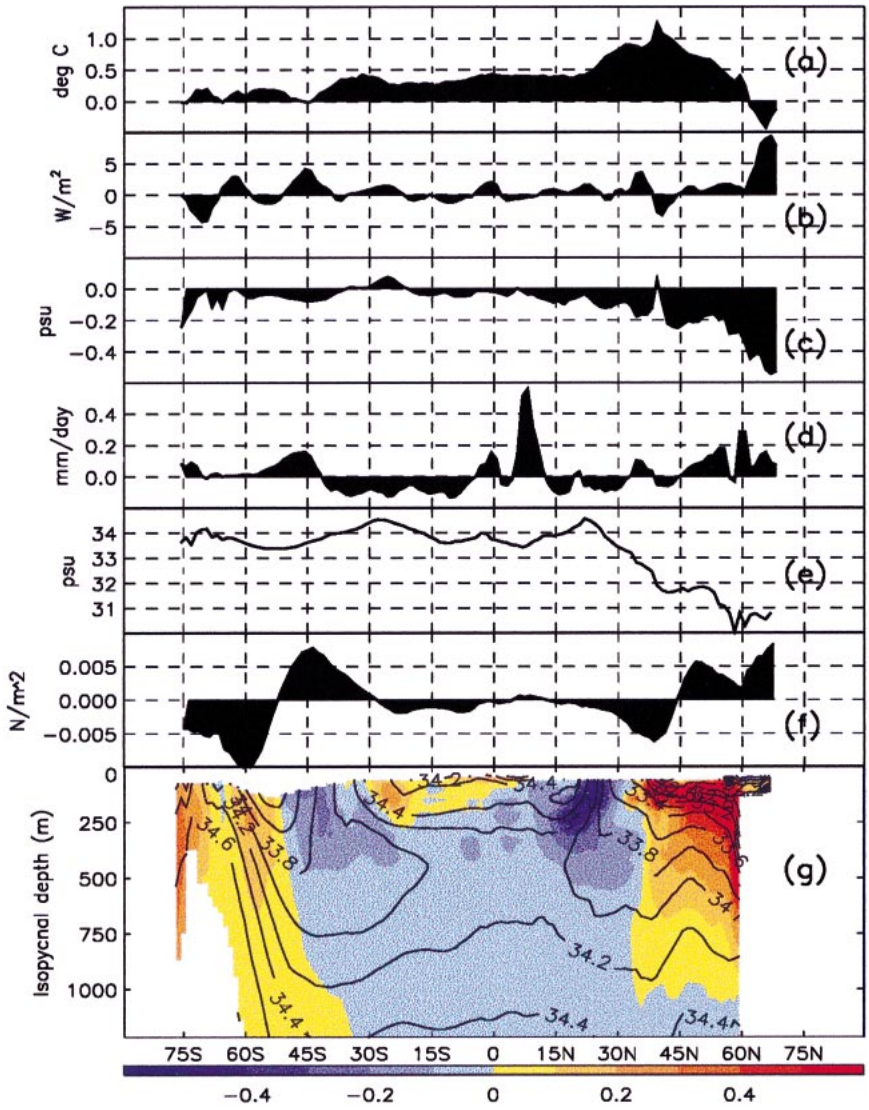

FIG. 7. Indo-Pacific zonal average in the HadCM3 model for the anthropogenic climate change scenario (B2) for (a) surface temperature change, (b) surface heat flux change, (c) surface salinity change, (d) surface freshwater input (precipitation plus runoff minus evaporation) change, (e) mean surface salinity, (f) zonal wind stress change, and (g) Indo-Pacific zonal average potential temperature change on isopycnals regridded onto pressure surfaces, with zonal average salinity field shown in contours. The changes are differences between the averages of 1989–98 and 2019–28.

duction, it is difficult from observations to piece together changes in surface fluxes with changes in the subsurface ocean properties, yet in the coupled model this should be possible. We will focus on the decades 1989–98 and 2019–28 in B2. There are two reasons for doing this: first, these were the decades used in the previous section to derive the fingerprint; second, we expect the signal over this time period to have a higher signal-to-noise ratio than currently observed, and it should therefore be easier to deduce the links between surface forcing and the subsurface pattern.

Figure 7a shows the zonal average change in surface temperature, which has increased at all latitudes, except north of 65°N. This suggests that the ocean has taken up heat. Figure 7b shows the zonal average change in the surface heat flux. This does not reveal such a uniform pattern and is most likely to be the result of surface heat flux being a particularly noisy field. Although the surface heat flux field is very noisy the average surface flux change over the Indo-Pacific region is approximately 0.4 W m^{-2}. For a swamp ocean 100 m thick, this heat flux over 30 yr would lead to a temperature change of 0.9°C, or about twice the sea surface temperature change of the model (Fig. 7a). The average

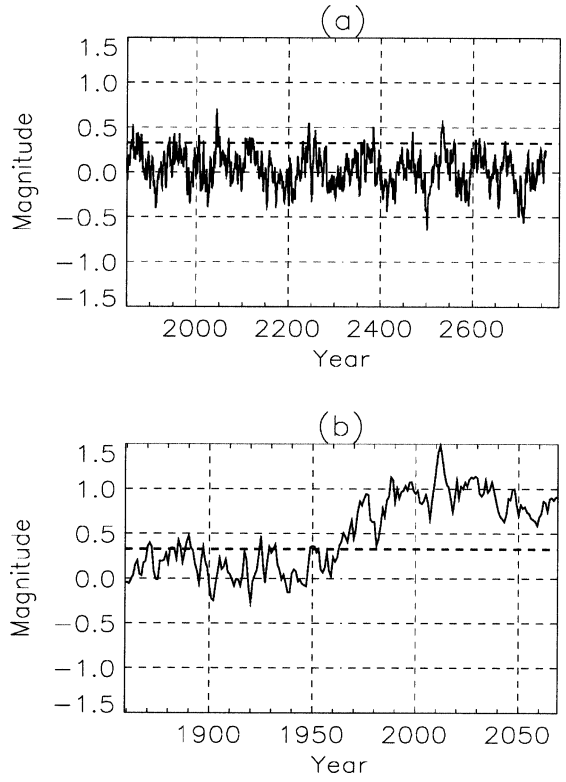

FIG. 8. Time series of the correlation of 30-yr changes in (a) CTL and (b) B2 projected onto the difference pattern from 2019 to 2028 minus 1989 to 1968. The 5% significance level from the CTL distribution is marked as the dashed line in both (a) and (b). Please note the different time axis in (a) and (b).

surface heat flux change implies a change in heat content of 9×10^{22} J over the Indo-Pacific region. The actual heat content change over the region is 16×10^{22} J. This difference cannot be accounted for by changes in the heat transported into the Indo-Pacific (this actually decreases by 0.02 PW). The discrepancy therefore implies that the time-integrated surface heat flux increase is actually larger than estimated by the differences between two periods (giving an average of 0.68 W m^{-2} over the Indo-Pacific). The uniformity of the sea surface temperature field (relative to the driving heat flux field) demonstrates the strong integrating response of the ocean to atmospheric forcing.

Similarly the ocean is a strong integrator of changes in precipitation. Figure 7c shows the zonal average change in surface salinity. The salinity changes shows freshening at all latitudes (except near 30°S). Figure 7d shows the zonal average change in surface freshwater input from precipitation, runoff, and evaporation. Precipitation (and runoff) has increased at high (poleward of 45°) and low (equatorward of 10°) latitudes, while evaporation has increased in midlatitudes in both hemispheres. As for temperature, it is not straightforward to draw parallels between changes in surface fluxes and changes in surface properties. In midlatitudes it may be the case that, as seen in the adjustment of CTL (PBGR), when the surface becomes warmer or fresher, greater stability inhibits vertical mixing (both wind driven and convective mixing). In this manner the surface properties will tend to be dominated by warming and freshening rather than cooling and salinification. Surface salinity (and temperature) may also be affected by changes in winds through changes in the surface Ekman transport as suggested by Rintoul and England (2002). Figure 7e shows the zonal surface salinity and hence its gradients. Northward Ekman transport is proportional to $-\tau_x/f$, where τ_x is the zonal wind stress and f is the Coriolis parameter. Increases in the zonal wind stress lead to an increase in equatorward Ekman transport. Figure 7f shows that there is an increase in the zonal wind stress in the Southern Hemisphere between 50° and 30°S, which drives fresher water into midlatitudes, while in the Northern Hemisphere there is an increase in zonal wind stress north of 45°N, which drives fresher water southward. Similarly, south of 50°S the zonal wind stress has decreased leading to a southward Ekman transport driving fresher surface waters to the north southward. Combined with the increase in precipitation minus evaporation ($P - E$) the surface waters in this region give a net decrease in salinity. The surface salinity signal at all latitudes ranges (except between 12° and 45°N) can be explained by the balance of Ekman transport of the preexisting surface salinity gradient and the changes in precipitation plus runoff minus evaporation.

Having examined the modeled changes in surface fluxes and the modeled change in subsurface properties, leads us to ask whether the two fit together to give a consistent picture. To do this we need to think about what combination of surface forcing can produce changes on isopycnals. If the water column is salty near the surface and fresher below (assuming that temperature is stably stratified), then adding cold or salty water at the surface will lead to warming on isopycnals. Alternatively, adding warm or freshwater at the surface will lead to cooling on isopycnals. If the water column is fresh near the surface and saltier below, then adding cold or freshwater at the surface will lead to cooling on isopycnals, while adding warm or salty water at the surface will lead to warming on isopycnals. The reader is referred to Figs. 1 and 2 from Bindoff and McDougall (1994) for further insight into these changes.

In the model we see warming on isopycnals south of 51°S (e.g., Figs. 5 and 7g). The water column is fresher near the surface and the θ–S diagram has a negative slope. Because the surface waters have both warmed and freshened the new near-surface θ–S curve is now displaced upward. On isopycnals, the temperature (and salinity) now appear warmer (and paradoxically saltier). For more detailed discussion of this response to changed surface waters see Bindoff and McDougall (1994). The precise contribution from the freshening and warming

of the surface waters can be solved using the methods of Bindoff and McDougall (1994, 2000).

Between 42° and 51°S, the θ–S relation still has a negative slope (i.e., just south of the core of the salinity minimum). However, the surface water properties are different. The surface temperature change is small in this latitude band (<0.1°C), while the surface salinity change is relatively large driven mainly by the large surface precipitation increase here. The increase in surface salinity displaces the θ–S curve downward (and to the left). On isopycnals the temperature (salinity) change is toward cooling and (freshening). This zone is the formation zone for Antarctic Intermediate Waters (AAIW).

Between 28° and 42°S the surface waters are warmer and saltier than the waters below (θ–S diagram has positive slope). The changes in surface water properties in this latitude band are toward warmer (0.5°C) water with slightly increased surface salinity ($\approx$0.005 psu). The increase in surface temperature displaces the new θ–S curve upward (and to the left). On isopycnals the temperature (salinity) is now paradoxically cooler (and fresher). This latitude band is the formation zone for SAMW. In the Tropics, between 3° and 28°S the θ–S curve has a negative slope above the shallow salinity maximum. The surface waters are much warmer (>0.25°C) than the relatively weak salinity decrease. Applying the same arguments as for south of 51°S on isopycnals the temperature (salinity) is now warmer (saltier).

Using the same arguments as in the Southern Hemisphere, in the Northern Hemisphere we see a similar pattern of modeled changes on isopycnals being driven by the changes in the surface water properties. Although the surface salinity decreases are large in the North Pacific, the surface temperature increases are also large and tend to dominate the water mass changes. This is because the North Pacific is a relatively warm ocean and the thermal expansion coefficient is much larger than the haline contraction coefficient. On a θ–S curve this means that the temperature changes are always moving the water mass properties farther along the temperature axis than the salinity decreases are moving water mass properties along the salinity axis.

The overall pattern of water mass change of the ocean interior for the 30-yr period from 1989–98 to 2019–28 is warming driven by the warmed surface waters. The only exception is the area in the formation zone of AAIW water (between 51° and 43°S), where the surface temperature increase is small (in density terms) and where the strong precipitation increase has made the surface salinity decrease relatively strong.

6. Discussion

The aims of this paper were threefold; to evaluate the response of the coupled model HadCM3 in the Indo-Pacific over the last 40 yr in terms of temperature and salinity changes, to understand which aspects of surface forcing drive the response in the interior ocean and to assess whether the large-scale pattern in the Indo-Pacific is a signature of anthropogenic climate change or whether it is simply a pattern that occurs as part of the internal variability of the coupled system.

In order to evaluate the modeled changes in temperature and salinity on isopycnals we developed a method to compare changes on a water mass axis. This method allowed a quantitative comparison to be made even when the basic temperature–salinity diagrams were only qualitatively the same. We envisage that this method could be used in other model–data comparisons to move toward quantitative evaluation of models. Using this method we were able to see that out of six sections throughout the Indo-Pacific, five of them showed good agreement between the modeled and observed changes. With just six sections, the emerging pattern was of a symmetric pattern of cooling (and freshening) on isopycnals in intermediate waters (i.e., salinity minimum and mode waters) of both hemispheres with warming on isopycnals near the surface.

The difficulties with looking at the changes on discrete sections are that we do not have the whole picture and the snapshot differences were taken at different times for each latitude. In the model, when we looked at the full two-dimensional picture of the changes between two decades (1959–68 and 1989–98) we saw a slightly different picture emerging—one of asymmetry between the two hemispheres—with the Southern Hemisphere showing the pattern of cooling on isopycnals, while the Northern Hemisphere is dominated by a pattern of warming on isopycnals. The later hydrographic sections at both 24° and 47°N were taken several years earlier than at more southerly latitudes (see Table 1) and it is plausible that the warming pattern may have been weaker at that stage in the Northern Hemisphere. In HadCM3, the asymmetric pattern is more likely to occur due to anthropogenic climate change but it is probably not a pattern that will exclusively dominate. By looking at a period when changes did not project strongly onto the asymmetric pattern, we found a symmetric pattern that, when projected onto the time series, appeared to be dominant under anthropogenic forcing. The strong similarity between the symmetric pattern and the observed changes suggests that the observed pattern is most likely to be a signature of anthropogenic climate change. It is interesting to note, however, that unlike our asymmetric pattern, the symmetric pattern did show signs of a weak low-frequency variability in the internal variability with a timescale of approximately 100 yr. If the model does provide a good representation of the real world, it may be the case that the phase of the symmetric mode in the internal variability may be enhancing the strength of the observed signal.

In the real world it is almost impossible to produce a self-consistent picture relating observed interior changes to observed surface fluxes. In a coupled model

this should be possible, yet often it can still be difficult to draw a coherent picture. In HadCM3 we have a picture where surface warming dominates the subsurface response at almost all latitudes except in the formation zone for Antarctic Intermediate Water where surface freshening (due to increased precipitation) is also important. Wind stress changes through Ekman transport are also important for driving changes in surface salinity.

In conclusion, the coupled model HadCM3 can simulate with reasonable skill interior ocean changes observed over the last 40 yr. The challenge for the future is to produce a dataset which is less limited in both spatial and temporal extent to further test coupled model simulations. In the case of the Indo-Pacific, our biggest uncertainty in the coupled model is in the response of the North Pacific. Further observations may help to characterize the interannual and interdecadal variability in that basin. We have shown that a symmetric pattern of warming on isopycnals at high latitudes and cooling on isopycnals at midlatitudes may be thought of as a fingerprint of anthropogenic forcing. Our biggest uncertainty in relation to the observations is that in the coupled model the symmetric pattern also occurred on a 100-yr timescale as part of internal variability. One caveat in our results is that we have only shown that this mode appears in the coupled model. This does not mean that this mode will necessarily appear in the real world. If this mode is real and it were subsequently found that the model estimate of internal variability is too low, it then becomes plausible that the observed water mass changes may be due to internal variability of the coupled system. Further observations are needed over the entire Indo-Pacific to monitor changes and assess the level of variability produced by coupled models used to predict changes in climate under anthropogenic forcing. The requirement for continued subsurface ocean observations may be partly met by the Argo project (an array of profiling floats; Wilson 2000), but repeat hydrographic sections may also be necessary to supplement the floats.

Acknowledgments. We thank Annie Wong for the analyzed hydrographic data from the Pacific Ocean and two reviewers for their comments. The work of HTB was carried out under DEFRA Contract PECD 7/12/37.

REFERENCES

Aoki, S., 1997: Trends and interannual variability of surface layer temperature in the Indian sector of the Southern Ocean observed by the Japanese Antarctic Research Expeditions. *J. Oceanogr.*, **53,** 623–631.

Banks, H. T., and R. A. Wood, 2002: Where to look for anthropogenic climate change in the ocean. *J. Climate,* **15,** 879–891.

——, ——, J. M. Gregory, T. C. Johns, and G. S. Jones, 2000: Are observed decadal changes in intermediate water masses a signature of anthropogenic climate change? *Geophys. Res. Lett.*, **27,** 2961–2964.

——, ——, and ——, 2002: Changes to Indian Ocean subantarctic mode water in a coupled climate model as CO_2 forcing increases. *J. Phys. Oceanogr.*, **32,** 2816–2827.

Barnett, T., D. Pierce, and R. Schnur, 2001: Detection of anthropogenic climate change in the world's oceans. *Science,* **292,** 270–274.

Bindoff, N. L., and J. A. Church, 1992: Warming of the water column in the southwest Pacific Ocean. *Nature,* **357,** 59–62.

——, and C. Wunsch, 1992: Comparison of synoptic and climatologically mapped sections in the South Pacific Ocean. *J. Climate,* **5,** 631–645.

——, and T. J. McDougall, 1994: Diagnosing climate change and ocean ventilation using hydrographic data. *J. Phys. Oceanogr.*, **24,** 1137–1152.

——, and ——, 2000: Decadal changes along an Indian Ocean section at 32°S and their interpretation. *J. Phys. Oceanogr.*, **30,** 1207–1222.

Bretherton, F. P., R. E. Davis, and C. B. Fandry, 1976: A technique for objective analysis and design of oceanographic experiments applied to MODE-73. *Deep-Sea Res.*, **23,** 559–582.

Cox, M. D., 1984: A primitive equation, three dimensional model of the ocean. Ocean Group Tech. Rep. 1, GFDL, Princeton, NJ, 143 pp.

Gent, P. R., and J. C. McWilliams, 1990: Isopycnal mixing in ocean circulation models. *J. Phys. Oceanogr.*, **20,** 150–155.

Gordon, A., E. J. Molinelli, and T. N. Baker, 1982: *Southern Ocean Atlas.* Columbia University Press, 35 pp. plus 248 pl.

Gordon, C., C. Cooper, C. A. Senior, H. Banks, J. M. Gregory, T. C. Johns, J. F. B. Mitchell, and R. A. Wood, 2000: The simulation of SST, sea ice extents and ocean heat transports in a version of the Hadley Centre coupled model without flux adjustments. *Climate Dyn.*, **16,** 147–168.

Guiot, J., J. J. Boreux, P. Braconnot, and F. Torre, 1999: Data-model comparison in paleoclimatology. *Climate Dyn.*, **15,** 569–581.

Houghton, J. T., Y. Ding, D. J. Griggs, M. Noguer, P. J. van der Linden, D. Xiaosu, and K. Maskell, Eds.,2001: *Climate Change 2001: The Scientific Basis.* Cambridge University Press, 881 pp.

Johns, T. C., R. E. Carnell, J. F. Crossley, J. M. Gregory, J. F. B. Mitchell, C. A. Senior, S. F. B. Tett, and R. A. Wood, 1997: The second Hadley Centre coupled ocean–atmosphere GCM: Model description, spinup and validation. *Climate Dyn.*, **13,** 103–134.

——, and Coauthors, 2001: Anthropogenic climate change for 1860 to 2100 simulated with the HadCM3 model under updated emissions scenarios. Hadley Centre Tech. Note 22, 61 pp.

Johnson, G. C., and A. H. Orsi, 1997: Southwest Pacific Ocean water-mass changes between 1968/69 and 1990/91. *J. Climate,* **10,** 306–316.

Levitus, S., and T. P. Boyer, 1994: *Temperature*. Vol. 4, *World Ocean Atlas 1994,* NOAA Atlas NESDIS 4, 117 pp.

——, and Coauthors, 1998: *Introduction.* Vol. 1, *World Ocean Database 1998,* NOAA Atlas NESDIS 18, 346 pp.

——, J. Antonov, J. Wang, T. Delworth, K. Dixon, and A. Broccoli, 2001: Anthropogenic warming of the earth's climate system. *Science,* **292,** 267–270.

Rintoul, S. R., and M. H. England, 2002: Ekman transport dominates local air–sea fluxes in driving variability of Subantarctic mode water. *J. Phys. Oceanogr.*, **32,** 1308–1321.

Roemmich, D., 1983: Optimal estimation of hydrographic station data and derived fields. *J. Phys. Oceanogr.*, **13,** 1544–1549.

Santer, B. D., U. Mikolajewicz, W. Bruggemann, U. Cubasch, K. Hasselmann, H. Hock, E. Maier-Reimer, and T. M. L. Wigley, 1995: Ocean variability and its influence on the detectability of greenhouse warming signals. *J. Geophys. Res.*, **100,** 10 693–10 725.

Wilson, S., 2000: Launching the Argo armada. *Oceanus,* **42,** 17–19.

Wong, A., N. L. Bindoff, and J. A. Church, 1999: Large-scale freshening of intermediate waters in the Pacific and Indian Oceans. *Nature,* **400,** 440–443.

——, ——, and ——, 2001: Freshwater and heat changes in the North and South Pacific Oceans between the 1960s and 1985–94. *J. Climate,* **14,** 1613–1633.